DIGITAL ACCESS TO SCHOLARSHIP AT HARVARD
DASH.HARVARD.EDU

HARVARD LIBRARY
Office for Scholarly Communication

Low Temperature Epitaxial Growth of High Permittivity Rutile \(TiO_2\) on \(SnO_2\)

Citation

Wang, Hongtao, Sheng Xu, and Roy G. Gordon. 2010. Low temperature epitaxial growth of high permittivity rutile \(TiO_2\) on \(SnO_2\). Electrochemical and Solid-State Letters 13(9): G75-G78.

Published Version

doi:10.1149/1.3457485

Permanent link

http://nrs.harvard.edu/urn-3:HUL.InstRepos:9962002

Terms of Use

This article was downloaded from Harvard University's DASH repository, and is made available under the terms and conditions applicable to Other Posted Material, as set forth at http://nrs.harvard.edu/urn-3:HUL.InstRepos:dash.current.terms-of-use#LAA

Share Your Story

The Harvard community has made this article openly available.
Please share how this access benefits you. Submit a story .

Accessibility

Electrochemical and Solid-State Letters, **13** (9) G75-G78 (2010)
1099-0062/2010/13(9)/G75/4/$28.00 © The Electrochemical Society

Low Temperature Epitaxial Growth of High Permittivity Rutile TiO_2 on SnO_2

Hongtao Wang,[a,z] Sheng Xu,[b] and Roy G. Gordon[b]

[a]*Institute of Applied Mechanics, Zhejiang University, Hangzhou 310027, China*
[b]*Department of Chemistry and Chemical Biology, Harvard University, Cambridge, Massachusetts 02138, USA*

Thin films of high dielectric constant ($\kappa \sim 68$) rutile phase titanium dioxide (TiO_2) were grown epitaxially on tin dioxide (SnO_2) substrates, which are a low cost, more abundant alternative to ruthenium electrodes used previously. Atomic layer deposition at low temperature (250°C) was used with titanium(IV) tetrakis(isopropoxide) and hydrogen peroxide (H_2O_2) as precursors. The rutile TiO_2 thin films have crystalline grains that match the structure and orientation of the grains in the polycrystalline rutile phase SnO_2 substrates. The epitaxial relations can be clearly identified from the continuous lattice fringes across the interfaces.
© 2010 The Electrochemical Society. [DOI: 10.1149/1.3457485] All rights reserved.

Manuscript submitted May 5, 2010; revised manuscript received June 7, 2010. Published June 29, 2010.

Metal-insulator-metal (MIM) structures with high capacitance density are increasingly needed for various applications in microelectronics,[1] capacitive energy storage,[2] and wireless communication with integrated radio-frequency circuits.[3] Great effort has been put into developing high dielectric constant (κ) materials as insulators, such as HfO_2 ($\kappa \sim 25$), ZrO_2 ($\kappa \sim 25$–30), Ta_2O_5 ($\kappa \sim 26$), and rare-earth oxides ($\kappa \sim 20$–30).[1,4,5] However, these oxides only have moderately high κ values, which cannot satisfy the demanding scaling of the effective oxide thickness (EOT) for the next-generation electronic devices.[6] Barium–strontium titanate $(Ba,Sr)TiO_3$ (BST) thin films are also of great interest for their possible ultrahigh dielectric constant ($\kappa \sim 300$),[1,7] but the BST dielectric constant has a strong thickness dependence and decreases to ~16 for a 20 nm thick film on a Ru bottom electrode.[8,9] It is also challenging to grow BST films on non-noble metal substrates. The IBM research group found that BST was amorphous on TaSiN barrier layers, whereas high-κ is only obtained for well-crystallized materials.[7] Recently, there has been extensive research on growing BST thin films on base-metal substrates to lower material cost.[10-12] Postdeposition annealing (400–750°C) in oxidizing ambient is necessary for making BST with a high dielectric constant,[12] but interfacial layers are introduced due to easy oxidation of base-metal electrodes, finally leading to a high EOT, which makes BST/base-metal stacks ineffective as well as complex to make.

Compared to the aforementioned oxides, the simple binary oxide, rutile phase TiO_2, is more attractive for its high dielectric constant (up to $\kappa \sim 114$ for films with random texture), less thickness dependence, and low dielectric loss.[13,14] However, TiO_2 thin films grown by both physical vapor deposition and chemical vapor deposition usually have anatase or amorphous structures, which only have a moderately high dielectric constant ($\kappa \sim 20$–40).[15] High temperature annealing (above 700°C) is necessary to transform them to the rutile phase, which requires high thermal budgets and causes structural integrity problems.[16] Atomic layer deposition (ALD) with halide-based precursors can deposit rutile-structured TiO_2, but residual halide impurity causes the films to have high leakage currents.[17] The as-deposited rutile TiO_2 films were realized only in a few systems with substrates such as oxidized noble metals (Ru and Ir) or RuO_2 [17] and insulating single-crystal oxides [sapphire(001) and MgO(001)].[4,18] These substrates have lattice planes matching rutile TiO_2 that make nucleation of the rutile phase kinetically preferable to the anatase phase.

In this article, we report, for the first time, ALD of rutile TiO_2 epitaxially on conductive SnO_2, which has potential application to high density capacitors. SnO_2 layers are ideal as bottom electrodes for several reasons: (*i*) SnO_2 has the rutile structure and small lattice mismatches to rutile TiO_2 [$(a_{TiO_2} - a_{SnO_2})/a_{SnO_2} = -3.10\%$, $(c_{TiO_2} - c_{SnO_2})/c_{SnO_2} = -7.16\%$]; (*ii*) SnO_2 thin films can be made highly conductive by doping with fluorine (F) or antimony (Sb) (<1 mΩ cm); (*iii*) SnO_2 is stable under the oxidizing annealing ambients needed for low leakage through high-κ insulators; and (*iv*) SnO_2 has low material cost compared to noble metal electrodes such as ruthenium or iridium.

Experimental

TiO_2/SnO_2 stacks were deposited in a flow-type ALD reactor operated at a base pressure of 0.3 Torr using N_2 as purging gas. The precursors are titanium(IV) tetrakis(isopropoxide) (TTIP) and hydrogen peroxide (H_2O_2) for TiO_2, and tetramethyl tin [$Sn(Me)_4$] and nitrogen dioxide (NO_2) for SnO_2.[19] The SnO_2 films were Sb-doped with antimony(III) ethoxide [$Sb(OEt)_3$].[20,21] All precursors are commercially available (e.g., Sigma-Aldrich) and inexpensive. The bubbler temperatures were 40 and 50°C for TTIP and $Sb(OEt)_3$, respectively. All other precursors were kept at room temperature. TiO_2 was deposited at a substrate temperature of 250°C by alternatively dosing the vapors from TTIP and H_2O_2. A trimethylaluminum dose was inserted every 90 cycles of TiO_2 to provide aluminum doping to decrease the leakage current. The conductive SnO_2 films were deposited by repeatedly growing 20 cycles of SnO_2 followed by one dose of $Sb(OEt)_3$ at a substrate temperature of 400°C. The growth rates are 0.3 and 1.2 Å/cycle for TiO_2 and SnO_2, respectively, independent of the substrate. The TiO_2/SnO_2 stack structure was characterized by transmission electron microscopy (TEM) and selected area diffraction (SAD). Capacitors for the measurement of the dielectric constant were made by evaporating palladium (Pd) electrodes and patterning capacitor areas lithographically by lift-off.

Results and Discussion

High resolution TEM was used to examine the epitaxial growth of rutile TiO_2 on an E-beam-evaporated SnO_2 substrate with grain size ~100 nm for the convenience of TEM imaging (Fig. 1a). The mass difference gives a clear contrast between TiO_2 (light color) and SnO_2 (dark color). The lattice fringes extend through the whole stack and are continuous across the interface. The atomic registry clearly shows that rutile TiO_2 grows epitaxially on SnO_2 at the low substrate temperature (250°C). Two lattice spacings, 0.35 and 0.24 nm, can be directly measured from the image, which are close to those of SnO_2(110) and SnO_2(200) planes. No difference in lattice spacing between TiO_2 and SnO_2 is observed in the high resolution image. The SAD pattern (Fig. 1b) has a fourfold symmetry and reveals the zone axis to be [001]. The major spots come from the SnO_2 crystal and are labeled according to the symmetry. The weak spots, indicated by arrows, distributed periodically around the major

[z] E-mail: htw@zju.edu.cn

Downloaded 23 Aug 2010 to 98.216.108.183. Redistribution subject to ECS license or copyright; see http://www.ecsdl.org/terms_use.jsp

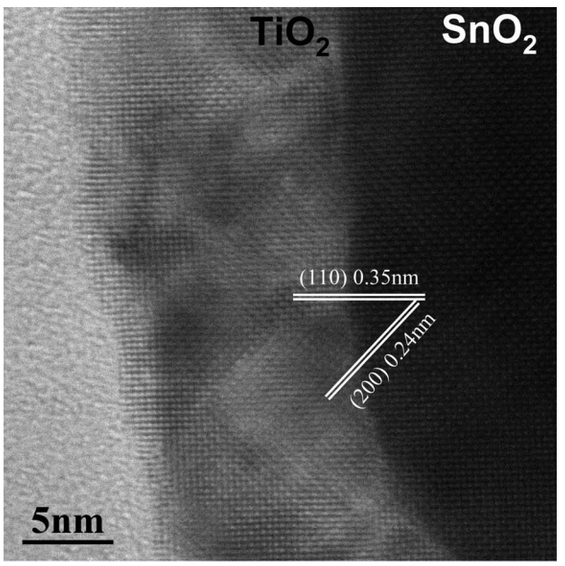

(a)

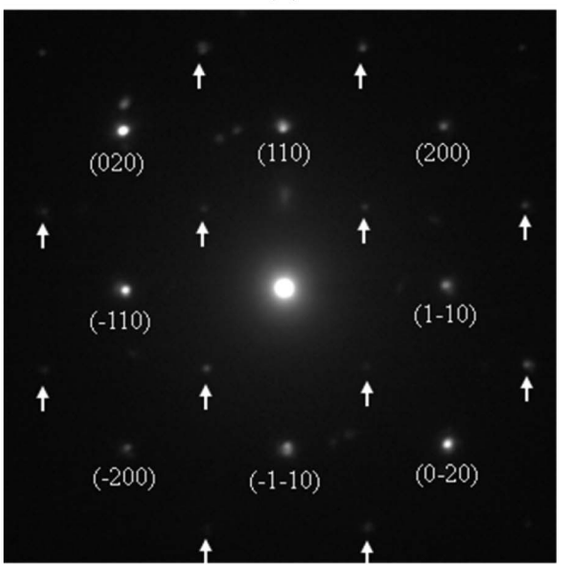

(b)

Figure 1. (a) High resolution cross-sectional TEM image of TiO_2/SnO_2 stack. The SnO_2 layer (200 nm) was deposited by electron-beam (E-beam) evaporation from bulk SnO_2 source followed by annealing in air for 1 h at 800°C. (b) The corresponding SAD pattern.

spots, come from the TiO_2 crystal and show the epitaxy relation to be $(110)TiO_2\|(110)SnO_2$:$[001]TiO_2\|[001]SnO_2$. Some random spots come from nearby grains due to the SAD aperture being larger than the grains and possibly also to astigmatism in the TEM.

The growth behavior of TiO_2 on conductive ALD SnO_2 is more interesting for applications. The as-deposited Sb-doped SnO_2 thin films are polycrystalline with grain size ~20 nm (Fig. 2). The inset SAD pattern has sharp and continuous rings, which indicate that the film has good crystallinity and random texture. The plan-view TEM image of a TiO_2/SnO_2 stack (Fig. 3a) shows that moiré fringes fully extend throughout each identifiable grain, which implies that both TiO_2 and SnO_2 films have comparable grain size. The corresponding SAD pattern is shown in Fig. 3b with Si(200) diffraction spots intentionally recorded as an internal scale for accurately measuring the

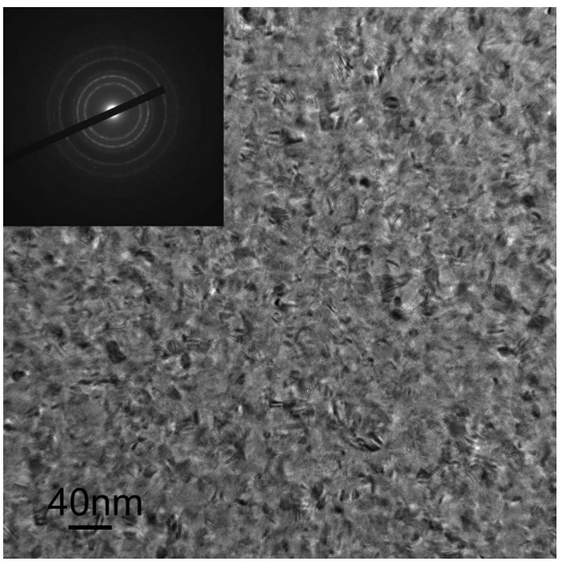

Figure 2. Plan-view TEM image of a 25 nm SnO_2 film on SiN_x membrane (50 nm) TEM grid. The inset is the SAD pattern.

lattice spacings. All rings can be unambiguously assigned to rutile phase SnO_2 and TiO_2 by comparing the lattice spacings to the powder X-ray diffraction database (PCPDF file no. 87-0920 and no. 88-0287). The anatase phase can be excluded by the absence of a diffraction ring from its (101) plane (3.51 Å, PCPDF file no. 89-4203), which has the maximum intensity and can be clearly distinguished from rutile TiO_2(110) (3.25 Å). Figure 4 confirms the local epitaxial growth of TiO_2 on the polycrystalline ALD SnO_2 layer, which also rules out the possible presence of anatase TiO_2 because of its large lattice mismatch with SnO_2. Similar SAD measurements in many parts of several samples ruled out the presence of any significant amount of anatase phase in the films.

Capacitors with the MIM structure were fabricated to characterize the electrical properties of the ALD TiO_2/SnO_2 stacks. Before the top Pd electrode evaporation, the stack was annealed at 300°C for 1 h in a flow of a mixture of O_2 and O_3 (concentration 5 g/N m^3). Ozone annealing is effective in filling the oxygen vacancies and lowering the leakage current.[22] Figure 5 shows the capacitance–voltage curve measured at 1 MHz for an 18 nm TiO_2 film. There is ~8% difference in capacitance between the applied negative and positive biases, which corresponds to the inversion and accumulation conditions of the Sb-doped SnO_2 layer, respectively. The equivalent SiO_2 thickness (EOT) is 0.98–1.07 nm and the dielectric constant is calculated to be 65–72, which is comparable to the dielectric constant of rutile TiO_2 deposited on oxidized ruthenium electrodes.[23] This high value of the dielectric constant corroborates the rutile structure of the TiO_2 films and the absence of the anatase phase, which would have a lower dielectric constant.

TiO_2 films grown under the same ALD conditions on other substrates, such as silicon and silicon dioxide, had the anatase crystal structure and a dielectric constant less than 40 (data not shown).

Conclusions

Rutile phase TiO_2 thin films were deposited by ALD on SnO_2 substrates at 250°C using TTIP and H_2O_2. The TiO_2 thin films have crystallinity matching that of the SnO_2 substrates. The epitaxial relations can be clearly identified from the lattice fringes that are continuous across the interfaces. High density (3.2–3.5 $\mu F/cm^2$) MIM capacitors were fabricated on planar substrates based on ALD

Downloaded 23 Aug 2010 to 98.216.108.183. Redistribution subject to ECS license or copyright; see http://www.ecsdl.org/terms_use.jsp

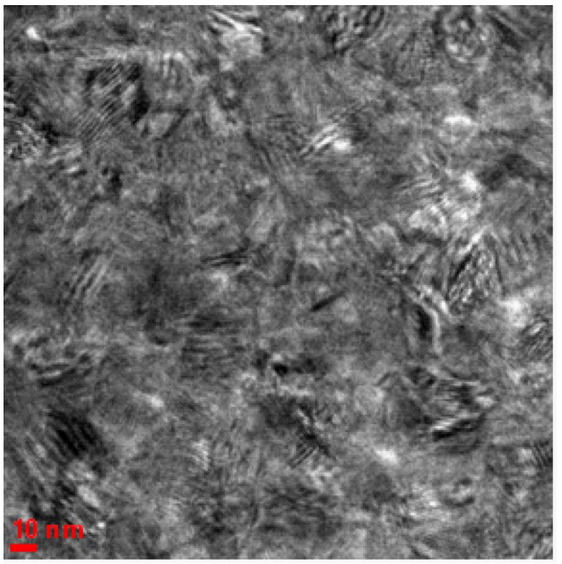

(a)

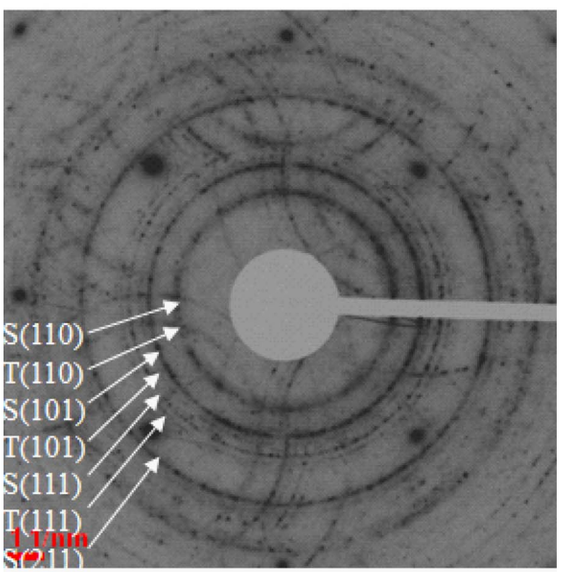

(b)

Figure 3. (Color online) (a) Plan-view TEM image of an 18 nm TiO_2/20 nm SnO_2 stack on Si substrate. (b) The SAD pattern. The discrete spots come from the electron diffraction by the Si substrate, which are doubly scattered by the polycrystalline film stack to form less intensive rings around each spot. In the label, S and T indicate rutile phase SnO_2 and TiO_2, respectively.

rutile TiO_2/SnO_2 stacks. The low thermal budget and the low material cost recommend ALD TiO_2/SnO_2 stacks as potential candidates for application to high density MIM capacitors.

Acknowledgments

This work was performed in part at Harvard University's Center for Nanoscale Systems, a member of the National Nanotechnology Infrastructure Network, supported by the U.S. National Science Foundation under award no. ECS-0335765. One of the authors acknowledges the support of the Science Foundation of Chinese University (grant no. 2009QNA4034).

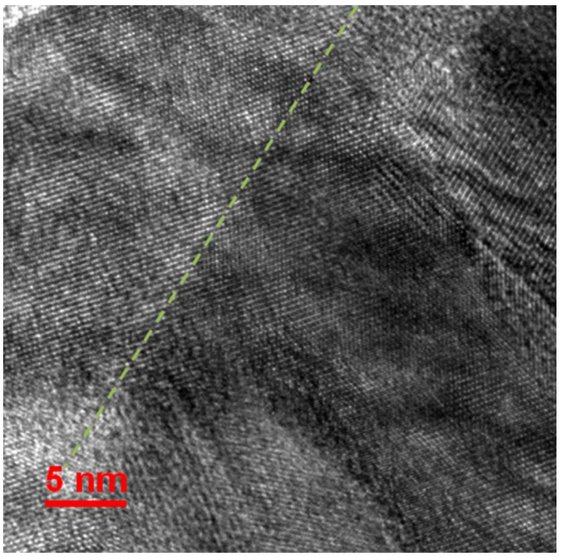

Figure 4. (Color online) Cross-sectional TEM image of a TiO_2/SnO_2 stack. The dashed lines indicate the interface.

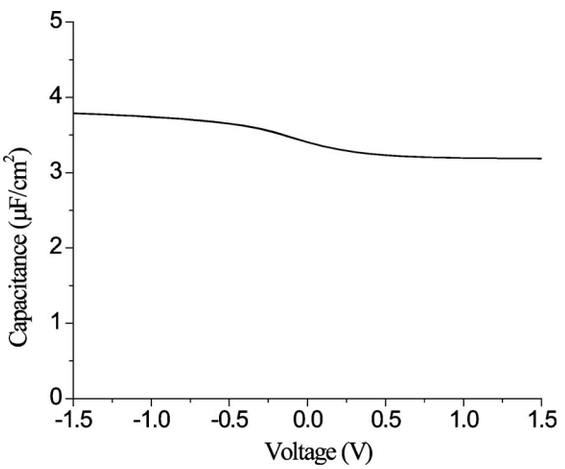

Figure 5. The capacitance density vs the applied voltage for the stack of Pd/TiO_2 (18 nm)/SnO_2.

References

1. G. D. Wilk, R. M. Wallace, and J. M. Anthony, *J. Appl. Phys.*, **89**, 5243 (2001).
2. P. Banerjee, I. Perez, L. Henn-Lecordier, S. B. Lee, and G. W. Rubloff, *Nat. Nanotechnol.*, **4**, 292 (2009).
3. S.-J. Ding, J. Xu, Y. Huang, Q.-Q. Sun, D. W. Zhang, and M.-F. Li, *Appl. Phys. Lett.*, **93**, 092909 (2008).
4. S. K. Kim, G. J. Choi, S. Y. Lee, M. Seo, S. W. Lee, J. H. Han, H. S. Ahn, S. Han, and C. S. Hwang, *Adv. Mater.*, **20**, 1429 (2008).
5. H. T. Wang, J. J. Wang, R. Gordon, J. S. M. Lehn, H. Z. Li, D. Hong, and D. V. Shenai, *Electrochem. Solid-State Lett.*, **12**, G13 (2009).
6. L. Jensen, P.-O. Astrand, and K. V. Mikkelsen, *J. Phys. Chem. B*, **108**, 8226 (2004).
7. D. E. Kotecki, J. D. Baniecki, H. Shen, R. B. Laibowitz, K. L. Saenger, J. J. Lian, T. M. Shaw, S. D. Athavale, C. Cabral, P. R. Duncombe, et al., *IBM J. Res. Dev.*, **43**, 367 (1999).
8. J.-H. Ahn, J.-Y. Kim, S.-W. Kang, J.-H. Kim, and J.-S. Roh, *Appl. Phys. Lett.*, **91**, 062910 (2007).
9. H. Tabata and T. Kawai, *Appl. Phys. Lett.*, **70**, 321 (1997).
10. P. Gonon and F. El Kamel, *J. Appl. Phys.*, **101**, 073901 (2007).
11. B. Laughlin, J. Ihlefeld, and J. P. Maria, *J. Am. Ceram. Soc.*, **88**, 2652 (2005).
12. A. V. Polotai, I. Fujii, D. P. Shay, G. Y. Yang, E. C. Dickey, and C. A. Randall, *J. Am. Ceram. Soc.*, **91**, 2540 (2008).
13. H. P. R. Frederikse, *Permittivity (Dielectric Constant) of Inorganic Solids: CRC Handbook of Chemistry and Physics*, CRC Press, Boca Raton, FL (2008).

Downloaded 23 Aug 2010 to 98.216.108.183. Redistribution subject to ECS license or copyright; see http://www.ecsdl.org/terms_use.jsp

14. R. A. Parker and J. H. Wasilik, *Phys. Rev.*, **120**, 1631 (1960).
15. S. A. Campbell, H. S. Kim, D. C. Gilmer, B. He, T. Ma, and W. L. Gladfelter, *IBM J. Res. Dev.*, **43**, 383 (1999).
16. D. J. Won, C. H. Wang, H. K. Jang, and D. J. Choi, *Appl. Phys. A: Mater. Sci. Process.*, **73**, 595 (2001).
17. K. Fröhlich, M. Ťapajna, A. Rosová, E. Dobročka, K. Hušeková, J. Aarik, and A. Aidla, *Electrochem. Solid-State Lett.*, **11**, G19 (2008).
18. M. Schuisky, A. Harsta, A. Aidla, K. Kukli, A. A. Kiisler, and J. Aarik, *J. Electrochem. Soc.*, **147**, 3319 (2000).
19. V. E. Drozd and V. B. Aleskovski, *Appl. Surf. Sci.*, **82–83**, 591 (1994).
20. A. G. Zawadzki, C. J. Giunta, and R. G. Gordon, *J. Phys. Chem.*, **96**, 5364 (1992).
21. J. Proscia and R. G. Gordon, *Thin Solid Films*, **214**, 175 (1992).
22. H. Shinriki, M. Nakata, Y. Nishioka, and K. Mukai, *IEEE Electron Device Lett.*, **10**, 514 (1989).
23. S. K. Kim, G. W. Hwang, W.-D. Kim, and C. S. Hwang, *Electrochem. Solid-State Lett.*, **9**, F5 (2006).

Downloaded 23 Aug 2010 to 98.216.108.183. Redistribution subject to ECS license or copyright; see http://www.ecsdl.org/terms_use.jsp